

Synthesis, Characterization, Electrochemistry, and Computational Studies of Ferrocenyl-Substituted Siloles

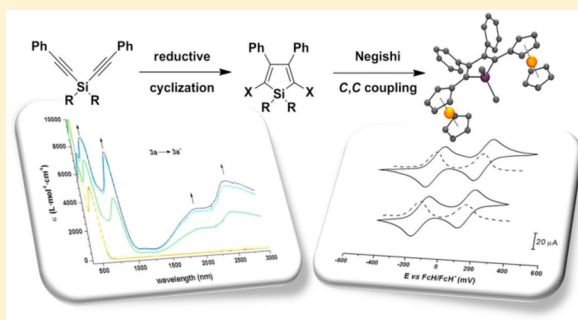
Steve W. Lehrich,[†] Alexander Hildebrandt,[†] Tobias Rüffer,[†] Marcus Korb,[†] Paul J. Low,^{‡,§} and Heinrich Lang^{*,†}

[†]Faculty of Natural Sciences, Institute of Chemistry, Inorganic Chemistry, Technische Universität Chemnitz, D-09107 Chemnitz, Germany

[‡]School of Chemistry and Biochemistry, University of Western Australia, Crawley, Perth, Western Australia, Australia

S Supporting Information

ABSTRACT: Ferrocenylsiloles of the type 2,5-Fc₂-3,4-Ph₂-C₄SiR₂ (**3a**, R = Me; **3b**, R = Ph) have been prepared by reductive cyclization from diethynylsilanes, followed by ferrocenylation using the Negishi C,C cross-coupling protocol with the silole ring serving as either the vinyl halogenide species or as the zinc organic component and the complementary functionality introduced on the ferrocenyl moiety. The electrochemical behavior of these silacyclic-bridged bis(ferrocenyl) complexes was investigated by cyclic and square wave voltammetry, and the nature of the redox products was studied by in situ UV–vis–near-IR spectroelectrochemical measurements. **3a,b** each undergo two sequential ferrocenyl-based redox processes, the separation of which ($\Delta E^{o'} = \Delta E_{2^{o'}} - \Delta E_{1^{o'}} = 300$ mV (**3a**), 280 mV (**3b**)) is in the range of structural similar systems such as 2,5-diferrocenyl-1-phenyl-1*H*-phosphole (280 mV) and 2,5-diferrocenylfuran (290 mV). Interestingly, the more electron rich silole **3b**, in comparison to **3a**, shows a modestly lower redox separation between the individual ferrocenyl oxidation processes, which may be due to the capacity of this group to shield the effect of an adjacent positive charge. An intervalence charge transfer (IVCT) absorption was found in the in situ NIR spectra of [**3a**]⁺ and [**3b**]⁺, the analysis of which is consistent with a moderate electronic interaction between the iron atoms through the *cis*-diene-like fragment of the silole bridge, allowing their description as Robin and Day class II mixed-valence systems. These conclusions are supported by results from quantum chemical calculations, which together with NMR studies of **3b**, also reveal the likely presence of a range of molecular conformations in solution.



INTRODUCTION

Silicon-containing metalloles (metallacyclopentadienes) are useful structural and electronic building blocks that can be used as monomers for the preparation of conjugated polymers^{1,2} or copolymers.^{3,4} For example, Tamao has presented a π -conjugated thiophene silole copolymer,⁵ while polysilole (PS) or silole-containing copolymers, which are linked through the 2,5-position, exhibit unique conductivity and semiconducting properties attributed to the small band gap (E_g),^{6–8} with computational studies indicating that PS has an even smaller band gap than other five-membered polyheterocycles such as polythiophene (PT, $E_g = 2.10$ eV) and polypyrrole (PP, $E_g = 2.85$ eV).^{7,10} These properties make silicon-containing metalloles interesting motifs for use in the design of organic semiconductors. In addition, due to the high electron mobility and high photoluminescence quantum yields, 1-silacyclopentadienes have attracted much interest for a diverse range of other materials applications such as new display devices or in organic light-emitting diodes (OLEDs), according to the interaction of the σ^* orbital of the Si–C bond with the π^* orbital of the butadiene fragment.^{11–14}

In order to gain a deeper insight into the electron transfer process that can be propagated through a single repeating unit of such polymers, and in light of our recent research on heterocyclopentadienes^{15–17} and aromatic five-membered heterocycles,^{18–23} we became interested in siloles as π -conjugated bridging units between two redox-active ferrocenyl termini. Herein, we present the synthesis and structural characterization of siloles of the type 2,5-Fc₂-3,4-Ph₂-C₄SiR₂ (R = Me, Ph), together with an electrochemical study of their redox chemistry and spectroelectrochemical investigation of the redox products. Computational calculations were carried out to enhance our understanding of the electronic structure of the compound in different oxidation states.

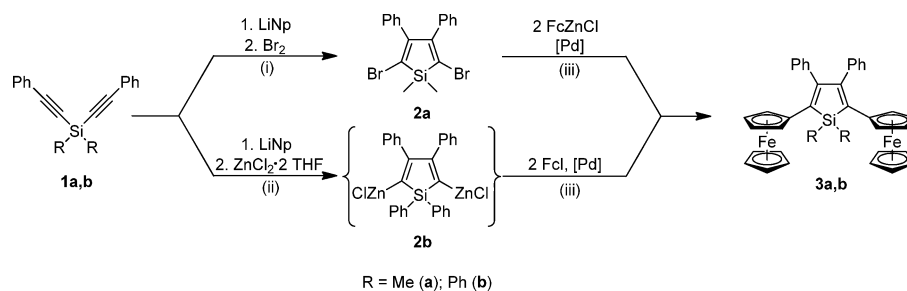
RESULTS AND DISCUSSION

Synthesis and Characterization. Silacyclopentadienes **2a,b** were synthesized by intramolecular reductive cyclization

Special Issue: Organometallic Electrochemistry

Received: January 23, 2014

Published: March 27, 2014

Scheme 1. Synthesis of 3a,b using Negishi Conditions^a

^aLegend: (i) tetrahydrofuran, 16 h, $-80\text{ }^{\circ}\text{C}$; (ii) tetrahydrofuran, 2 h, room temperature; (iii) tetrahydrofuran, [Pd] = $[\text{Pd}(\text{CH}_2\text{CMe}_2\text{P}^t\text{Bu}_2)(\mu\text{-Cl})_2]$ (0.25 mol %), $80\text{ }^{\circ}\text{C}$, 2 days. Abbreviations: LiNp, lithium naphthalenide; Fc, $\text{Fe}(\eta^5\text{-C}_5\text{H}_4)(\eta^5\text{-C}_5\text{H}_5)$.

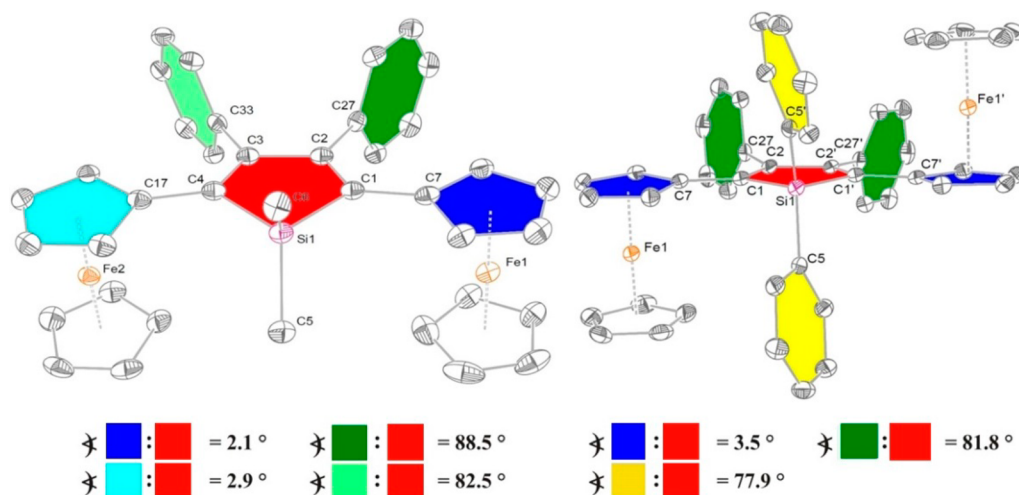


Figure 1. ORTEP diagram (50% probability level) of the molecular structures of 3a (left) and 3b (right) with the atom-numbering scheme. The sign \angle indicates interplanar angles between calculated mean planes of atoms adjoining differently colored areas. All hydrogen atoms have been omitted for clarity. Selected bond distances (Å) and angles (deg), and torsion angles (deg): 3a, Si1–C1 = 1.8787(16), C1–C2 = 1.359(2), C1–C7 = 1.463(2), Si1–C4 = 1.8817(16), Si1–C5 = 1.8710(17), Si1–C6 = 1.8692(17), C2–C3 = 1.498(2), C2–C27 = 1.494(2), C3–C33 = 1.494(2), C3–C4 = 1.360(2), C4–C17 = 1.462(2), average D–Fe = 1.649, C2–C1–Si1 = 107.31(11), C1–Si1–C4 = 92.26(7), average D–Fe–D = 177.43; 3b, Si–C1 = 1.871(4), C1–C2 = 1.353(5), C1–C7 = 1.463(5), Si1–C5 = 1.870(3), C2–C2A = 1.507(6), C2–C27 = 1.491(5), average D–Fe = 1.648, C2–C1–Si1 = 107.0(2), C1–Si1–C1A = 93.0(2), average D–Fe–D = 177.4. D denotes the centroid of C_5H_4 or C_5H_5 . Symmetry operation for generating equivalent atoms: ($'$) $-x + 1/2, y, -z + 5/2$.

from dimethylbis(phenylethynyl)silane (**1a**) and diphenylbis(phenylethynyl)silane (**1b**) with lithium naphthalenide followed by bromination with elemental bromine, forming dibromide **2a**, or the reaction with $[\text{ZnCl}_2 \cdot 2\text{thf}]$ giving the organozinc species **2b** (Scheme 1). Applying Negishi-ferrocenylation conditions, the reaction of **2a** with FcZnCl (Fc = $\text{Fe}(\eta^5\text{-C}_5\text{H}_4)(\eta^5\text{-C}_5\text{H}_5)$) as the ferrocenyl source and $[\text{Pd}(\text{CH}_2\text{CMe}_2\text{P}^t\text{Bu}_2)(\mu\text{-Cl})_2]$ as the precatalyst gave silole **3a**. The analogous coupling of 2,5-Br₂-3,4-Ph₂-C₄SiPh₂ with ferrocenylzinc chloride did not result in the formation of the desired **3b**. The synthesis of **3b** was realized by a Negishi C,C cross-coupling reaction using iodoferrocene as the ferrocenyl source, while the application of bromoferrocene was unsuccessful. After the appropriate workup (Experimental Section), molecules **3a,b** were obtained in moderate (**3a**) to low (**3b**) yield as dark red solids.

Siloles **3a,b** are stable toward air, light, and moisture in the solid state and in solution and were characterized by elemental analysis, UV–vis, IR, and NMR (^1H , $^{13}\text{C}\{^1\text{H}\}$, $^{29}\text{Si}\{^1\text{H}\}$) spectroscopy, and mass spectrometry. The molecular structures of **3a,b** in the solid state were determined by single-crystal X-ray structure analysis. The electrochemical behavior of **3a,b** was

examined by cyclic voltammetry (CV), square wave voltammetry (SWV), and in situ UV–vis–near-IR spectroelectrochemistry. Furthermore, DFT calculations were carried out to support the conclusions drawn from the spectroscopic measurements and enhance the understanding of the underlying electronic structures of $[\mathbf{3a,b}]^{n+}$ ($n = 0-2$).

The ^1H NMR spectra of **3a,b** show the characteristic pattern for the two equivalent ferrocenyl groups with one singlet (C_5H_5) and two pseudotriplets (C_5H_4) with $J = 1.90$ Hz, the latter being characteristic for AA'XX' spin systems.²⁴ The signal of the C_5H_5 group is found at 4.06 ppm for **3a** and 3.52 ppm for **3b**. The $^{13}\text{C}\{^1\text{H}\}$ and $^{29}\text{Si}\{^1\text{H}\}$ NMR spectra show typical resonances corresponding to the heterocyclic core and the methyl and the phenyl groups (Experimental Section).²⁵ High-resolution mass spectrometry (HRMS) displays an anticipated m/z peak of 630.1298 for **3a** and 754.1425 for **3b**.

Single crystals of **3a** and of **3b** in the form $\mathbf{3b} \cdot 2\text{CH}_2\text{Cl}_2$ suitable for X-ray diffraction analysis could be obtained by diffusion of n -hexane into a dichloromethane solution containing either **3a** or **3b** at ambient temperature. The molecular structures of **3a,b** in the solid state together with

stabilization energies of 9–12 kJ mol⁻¹ for the benzene dimer.²⁶ Furthermore, in contrast to the case for 2,3,4,5-tetraferrocenyl-*N*-phenyl-1-*H*-pyrrole¹⁹ the activation entropy of the ferrocenyl rotation in **3b** is positive. This is generally the case when the transition state exhibits more degrees of freedom than the ground state. The π interaction not only hinders the rotation of the ferrocenyls but also limits the freedom of rotation for the C₅H₅ rings and the phenyl groups. Therefore, the ground states of the rotation around the silole–ferrocenyl carbon–carbon bond could be considered entropically unfavorable, hence resulting in a positive activation entropy. The observations of dynamic NMR studies not only support the crystallographically determined π interaction, but also showed that even in solution, especially at low temperatures, a rotation barrier of the ferrocenyls is present and should be taken into consideration. Please note that, due to the absence of a π interaction in **3a**, no rotation barrier could be observed at temperatures down to -100 °C (Supporting Information, Figure SI17).

Electrochemistry. The electrochemical properties of **3a,b** were investigated by cyclic voltammetry (CV) and square wave voltammetry (SWV) (Figure 4), and the nature of the redox

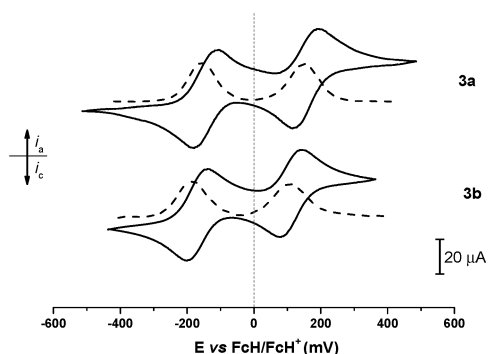


Figure 4. Cyclic voltammograms (solid lines) and square wave voltammograms (dotted lines) of **3a,b** in dichloromethane solutions (1.0 mmol L⁻¹) at 25 °C (scan rate 100 mV s⁻¹; supporting electrolyte 0.1 mol L⁻¹ of [NⁿBu₄][B(C₆F₅)₄]).

products was explored in more detail by in situ UV–vis–near-IR spectroelectrochemistry (Figure 5). The voltammetric measurements were carried out in dry dichloromethane solutions of [NⁿBu₄][B(C₆F₅)₄] (0.1 mol L⁻¹), the latter being chosen to minimize ion pairing effects^{34–36} (for examples of the application of [NⁿBu₄][B(C₆F₅)₄] as supporting electrolyte within electrochemical measurements see refs 15, 19, 22, and 37–41). Cyclic voltammetry studies were performed at 25 °C with a scan rate of 100 mV s⁻¹. All potentials are referenced to the FcH/FcH⁺ (FcH = Fe(η^5 -C₅H₅)₂) redox couple ($E^{o'} = 0.0$ mV).⁴²

The ferrocenyl substituents in **3a,b** are oxidized separately, showing two reversible redox events with redox separations ($\Delta E^{o'} = \Delta E_2^{o'} - \Delta E_1^{o'}$) of 300 mV (**3a**) and 280 mV (**3b**), respectively, which indicates some through-bond or through-space electronic interactions between the ferrocenyl/ferrocenium termini (Table 1, Figure 4). While for 1,1-dimethyl-2,3,4,5-tetraphenylsilacyclopentadiene irreversible oxidation ($E_{pa} = 1482$ mV) and reduction ($E_{pc} = -2174$ mV) processes have been observed by Tracy,³¹ compounds **3a,b** showed no such redox events within the measured potential range (-2500 to 1800 mV). Within the series of bis(ferrocenyl) complexes featuring five-membered aromatic heterocyclic bridges, such as **5**,³⁶ **7**,³⁵ and **8**¹⁹ (Chart 1), it could be shown that the

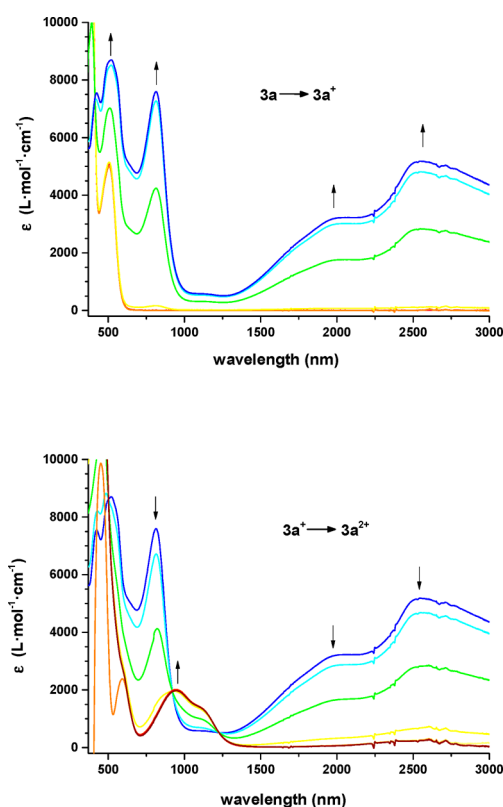


Figure 5. UV–vis–near-IR spectra of [3a]ⁿ⁺ ($n = 0–2$) in dichloromethane solution (2.0 mmol L⁻¹) at increasing potentials (vs Ag/AgCl): (top) -200 to 300 mV; (bottom) 300 to 700 mV at 25 °C. The supporting electrolyte was 0.1 mol L⁻¹ of [NⁿBu₄][B(C₆F₅)₄]. Arrows indicate an increase or decrease in the absorptions.

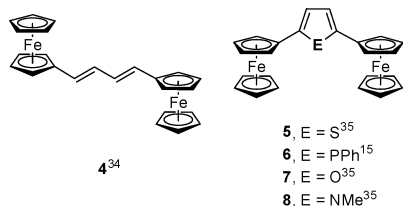
Table 1. Cyclic Voltammetry Data of **3a,b** and **4–8** for Comparison

| compd | $E_1^{o'}$ (mV) ^a (ΔE_p (mV)) ^c | $E_2^{o'}$ (mV) ^b (ΔE_p (mV)) ^c | $\Delta E^{o'}$ (mV) ^d |
|--------------------------|--|--|-----------------------------------|
| 3a ^e | -145 (72) | 155 (74) | 300 |
| 3b ^e | -170 (64) | 110 (68) | 280 |
| 4 ^{f,43} | -35 | 90 | 225 |
| 5 ^{e,44} | -94 (65) | 166 (65) | 260 |
| 6 ^{e,15} | -110 (72) | 170 (80) | 280 |
| 7 ^{e,44} | -152 (60) | 138 (63) | 290 |
| 8 ^{e,44} | -206 (65) | 204 (65) | 410 |

^a $E^{o'}$ = formal potential of first redox process. ^b $E^{o'}$ = formal potential of second redox process. ^c ΔE_p = difference between oxidation and reduction potentials. ^d $\Delta E^{o'}$ = potential difference between the two ferrocenyl-related redox processes. ^eConditions: potentials vs FcH/FcH⁺, scan rate 100 mV s⁻¹ at a glassy-carbon electrode of 1.0 mmol L⁻¹ solutions in dry dichloromethane containing 0.1 mol L⁻¹ of [NⁿBu₄][B(C₆F₅)₄] as supporting electrolyte at 25 °C. ^fConditions: measured in [NⁿBu₄][B(3,5-C₆H₃(CF₃)₂)] (0.1 M) in dichloromethane with a Pt working electrode and Ag/AgI reference electrode, referenced to FcH/FcH⁺, at a scan rate 50 mV/s.

separation of the two ferrocenyl redox waves depends on the electronic characteristics of the bridging moiety. The more electron-rich the bridging group, the lower (less positive) the first ferrocenyl oxidation ($E_1^{o'}$) potential process becomes, and hence electron-rich heterocycles show higher $\Delta E^{o'}$ values (Table 1). The ^cC₄Si bridging unit within silole **3b** donates more electron density toward the ferrocenyl moieties in comparison with **3a**, and thus those ferrocenyls are more

Chart 1. Selected Diferrocenyl Molecules for Comparison



easily oxidized (**3a**, $E_1^{o'}$ = -145 mV; **3b**, $E_1^{o'}$ = -170 mV); however, **3b** possesses a lower redox separation (**3a**, 300 mV; **3b**, 280 mV), which is in contrast to the trends revealed by other species in this five-membered heterocyclic family (Table 1). The discrepancy between the observed and expected electrochemical behavior of **3a,b** might be explained by the influence of the cross-hyperconjugation of the SiMe₂ moiety to the butadiene system.^{12,46–49} Due to the involvement of the silicon atom in the π conjugation, the electronic interactions between the respective iron centers might be increased, leading to some additional stabilization of the mono-oxidized redox product [**3a**]⁺ relative to [**3b**]⁺. In order to explore this hypothesis, the IVCT transitions within the mixed-valent cations [**3a**]⁺ and [**3b**]⁺ have been studied using spectroelectrochemical methods.

Spectroelectrochemistry. Spectroelectrochemical studies were performed in an optically transparent thin-layer electrochemistry (OTTLE) cell containing 2.0 mmol L⁻¹ of **3a** or **3b** and 0.1 mol L⁻¹ of [NⁿBu₄][B(C₆F₅)₄] as the supporting electrolyte, with stepwise increase of the applied potential from -200 to 700 mV vs Ag/AgCl. The potential was increased using varying step heights of 25, 50, and 100 mV. This procedure allowed the sequential in situ generation of [**3a,b**]⁺ and [**3a,b**]²⁺ (Figure 5). In their charge-neutral, Fe(II/II) state, siloles **3a,b** are, as expected, transparent in the near-IR region, while broad intense transitions (IVCT and LMCT) could be observed as **3a,b** were oxidized to [**3a**]⁺ and [**3b**]⁺ by increasing the applied potential. Deconvolution of this absorption envelope required four Gaussian-shaped spectral components, consistent with an IVCT transition at 4700 cm⁻¹ ([**3a**]⁺) or 4650 cm⁻¹ ([**3b**]⁺) ([**3a**]⁺, ϵ_{\max} = 3150 L mol⁻¹ cm⁻¹, $\Delta\nu_{1/2}$ = 2950 cm⁻¹; [**3b**]⁺, ϵ_{\max} = 2270 L mol⁻¹ cm⁻¹, $\Delta\nu_{1/2}$ = 3310 cm⁻¹) and two LMCT bands at 3470 and 4000 cm⁻¹ ([**3a**]⁺) and 3460 and 3930 cm⁻¹ ([**3b**]⁺) (Table 2 and Figure 6). The fourth component was used to simulate the low-energy edge of higher energy absorptions that protrude into the near-IR region. Due to the sp³ character of the silicon atom, the silole fragment ^cC₄Si is rather comparable to a *cis*-diene system.⁴³ However, the intensity of the IVCT absorption found in [**3a**]⁺ exceeds those found in mixed valence [**6**]⁺¹⁵ and [**4**]⁺⁴³ while the IVCT characteristics (ϵ_{\max} , $\Delta\nu_{1/2}$) of [**3b**]⁺ are very similar

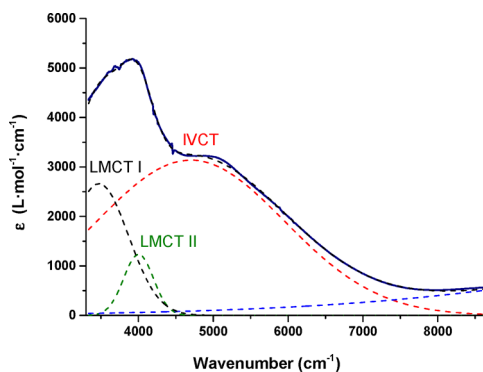


Figure 6. Four-band Gaussian deconvolution of the near-IR absorption envelope of [**3a**]⁺ obtained by spectroelectrochemistry in an OTTLE cell.

to those of the diene analogue [**4**]⁺. The higher extinction coefficient of the IVCT absorption in [**3a**]⁺ might be a consequence of cross-hyperconjugation of the SiMe₂ building block with the butadiene unit causing involvement of the sp³-hybridized silicon atom in the π -conjugated system, a phenomenon that has been described in, for example, methyl- and H-substituted siloles.^{12,46–49} The fact that the IVCT transition associated with [**3b**]⁺ is less intense and broader than that of [**3a**]⁺ demonstrates a weaker electronic coupling between the redox centers. In support of this, we note that although $\Delta E^{o'}$ depends on many factors, including ion-pairing energies, solvation factors, magnetic effects, and metal–ligand bonding variations in different oxidation states, in addition to statistic and electrostatic terms,^{50,51} these are not expected to be substantively different in **3a**/[**3a**]⁺ vs **3b**/[**3b**]⁺. Hence, the smaller $\Delta E^{o'}$ value observed for **3b** (see Electrochemistry) is also consistent with a smaller contribution of the resonance term. Comparison of the characteristics of the IVCT transition of [**3a**]⁺ and [**3b**]⁺ with those from other aromatic five-membered heterocycles revealed that the $\Delta\nu_{1/2}$ values for [**5**]⁺,^{21,45,52} [**6**]⁺,¹⁵ [**7**]⁺,⁴⁴ and [**8**]⁺^{44,53,54} are smaller (2300–2400 cm⁻¹) than those of [**3a**]⁺ and [**3b**]⁺, while the intensities are within the same range. Phosphole [**6**]⁺,¹⁵ which is similar to siloles **3a,b**, also contains a nonaromatic five-membered heterocycle showing IVCT absorptions with $\Delta\nu_{1/2}$ values comparable to [**3a**]⁺ and [**3b**]⁺, respectively.

The electronic coupling parameter H_{ab} can be calculated according to Hush's two-state model for a class II system as shown in eq 1, where r_{ab} is the effective electron transfer

$$H_{ab} = 2.06 \times 10^{-2} \frac{\sqrt{\nu_{\max} \epsilon_{\max} \Delta\nu_{1/2}}}{r_{ab}} \quad (1)$$

Table 2. Near-IR Data of the Absorptions of Siloles [**3a**]⁺ and [**3b**]⁺ ^a

| compd | ν_{\max} (cm ⁻¹) (ϵ (L mol ⁻¹ cm ⁻¹)) | $\Delta\nu_{1/2}$ (cm ⁻¹) | $\Delta\nu_{1/2}$ (theor) (cm ⁻¹) | H_{ab} (syn conformation) (cm ⁻¹) ^b | H_{ab} (anti conformation) (cm ⁻¹) ^b | |
|------------------------|--|---------------------------------------|---|--|---|-----|
| 3a ⁺ | IVCT | 4700 (3150) | 2950 | 3300 | 542 | 500 |
| | I LMCT | 3470 (2650) | 950 | | | |
| | II LMCT | 4000 (1250) | 450 | | | |
| 3b ⁺ | IVCT | 4650 (2250) | 3300 | 3300 | 482 | 445 |
| | I LMCT | 3460 (1450) | 800 | | | |
| | II LMCT | 3930 (800) | 450 | | | |

^aConditions: in dry dichloromethane containing 0.1 mol L⁻¹ of [NⁿBu₄][B(C₆F₅)₄] as supporting electrolyte at 25 °C. ^b H_{ab} was calculated according to eq 1 with r_{ab} (syn) = 7.9438 Å and r_{ab} (anti) = 8.6074 Å.

distance between the two redox-active sites, which is notoriously hard to determine experimentally.^{51,55–58} Therefore, the crystallographic Fe–Fe distances were used to estimate H_{ab} . Since the ferrocenyl substituents within **3a,b** can adopt both syn and anti conformations, H_{ab} was calculated using crystallographic data derived from **3a** representing the syn orientation ($r_{ab}(\text{syn}) = 7.9438(18)$ Å) and anti-oriented **3b** ($r_{ab}(\text{anti}) = 8.6074(9)$ Å). Please note that the effective electron transfer distance is expected to be shorter than the geometric Fe–Fe distances and hence H_{ab} might be underestimated.⁵⁴ As expected, due to the lower r_{ab} value, H_{ab} is higher for the syn conformation for both molecules [**3a**]⁺ and [**3b**]⁺, in comparison with the respective anti conformer (Table 2). Silole [**3a**]⁺ exhibits higher H_{ab} values in comparison with [**3b**]⁺; nevertheless, the determined values are quite similar, showing that there are only minor differences in the electronic coupling caused by the different substitution on the silicon atom.

The unexpectedly strong IVCT interactions allowed classification of siloles [**3a**]⁺ and [**3b**]⁺ as moderately and moderately to weakly coupled class II systems, respectively, according to the classification system introduced by Robin and Day.⁵⁸

Further oxidation of [**3a**]⁺ and [**3b**]⁺ to the dications [**3a**]²⁺ and [**3b**]²⁺ leads to a disappearance of the IVCT bands as homovalent Fe(III/III) species are formed. In association with this, two MLCT transitions emerge at ca. 1000 nm (10000 cm⁻¹). The LMCT bands that are determined for [**3a**]⁺ and [**3b**]⁺ can also be found in dications [**3a**]²⁺ and [**3b**]²⁺, exhibiting a decreased intensity (ca. 200 L mol⁻¹ cm⁻¹) (Supporting Information).

Computational Studies. To explore the electronic structures of [**3a,b**]ⁿ⁺ ($n = 0–2$) in more detail, the computational model systems *syn*-[**3a'**]ⁿ⁺, *anti*-[**3a'**]ⁿ⁺, and *anti*-[**3b'**]ⁿ⁺ (where the prime (') nomenclature is introduced to distinguish the computational from the real system) were analyzed (B3LYP using Dunning's all-electron valence double- ζ (D95 V) for C and H atoms and the Los Alamos ECP/double- ζ valence basis set on Fe and Si (LANL2DZ) and a CPCM-dichloromethane solvent model). Tables giving orbital energies and compositions are available in the Supporting Information, together with the results from benchmarking studies carried out on **3a'** using 3-21G* (all atoms) and 6-31G** (H, C, Si)/LANL2DZ (Fe) basis sets, which reveal no structural or electronic differences of any significance to the results reported in the main body of the paper.

The optimized geometry of *syn*-**3a'** compares very well with that determined crystallographically for **3a** (Figure 7 and Table 3) and differs little from that of *anti*-**3a'**, which lies only +0.37 kJ/mol lower in energy. The optimized geometries of the syn and anti conformers of **3a'** both exhibit pronounced bond-

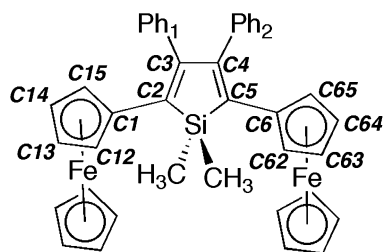


Figure 7. Atom-labeling scheme of **3a**.

length alternation in the silacyclopentadiene ring and significant *cis*-diene-like character in the bridging moiety linking the two ferrocenyl fragments, in a manner entirely analogous to the crystallographically determined structures of **3a,b** and other heterocyclic bridged bis(ferrocenyl) complexes. In both the computational models and the crystallographically determined structures, the C1–C15, silacyclopentadiene, and C6–C65 rings are essentially coplanar, while the geometry at Si is distorted from idealized tetrahedral by the inclusion within the C₄Si ring. The HOMO of *syn*-**3a'** features a substantial (ca. 42%) character from the *cis*-butadiene-like portion of the silacycle, admixed with contributions from the ferrocenyl substituents (ca. 28% each) (Figure 8). There is negligible contribution from both the SiMe₂ fragment and the phenyl groups, the latter being oriented approximately perpendicularly to the plane of the silacycle. The electronic structure varies little as a function of the relative disposition of the ferrocenyl moieties across the silacyclic ring, and the composition and energy of the frontier orbitals of the anti conformer *anti*-**3a** are essentially the same as those described for the syn form (Supporting Information).

The monocation *syn*-[**3a'**]⁺ displays a number of structural and orbital features that are entirely consistent with the description of this species as an Fe(II/III) mixed-valence (MV) complex. The C1–C2 bond is rather shorter in the monocation (1.445 Å) than in the neutral species (1.467 Å), although the C5–C6 bond lengths are more consistent between the two oxidation states (**3a'**, 1.467 Å; [**3a'**]⁺, 1.458 Å), while within the silacyclopentadiene ring the bond length alternation is modestly less pronounced (Table 3), giving rise to a valence bond description with more cumulenic character in the diene-like backbone. There is also a substantial elongation of the Fe–Cp₁ distance in [**3a'**]⁺ in comparison with **3a'**, consistent with the oxidation of this site (Table 3). However, there is little variation in the local geometry at the silicon center. The composition of the molecular orbitals also supports the MV description of [**3a**]⁺, with the β -LUSO in [**3a'**]⁺ essentially localized (80%) on one ferrocenyl center and a small contribution (14%) from the diene-like backbone (Figure 9), while the β -HOSO has more character derived from the other ferrocenyl moiety (58%) and the diene (30%) with 10% arising from the formally oxidized ferrocenyl center (Figure 10).

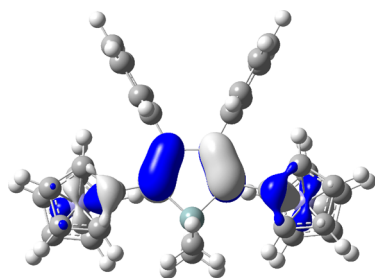
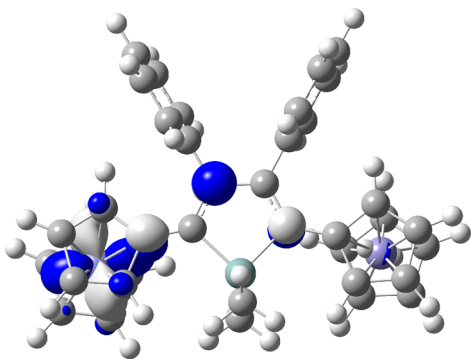
Interestingly, *anti*-[**3a'**]⁺ is essentially isoenergetic with the syn isomer, lying barely 0.65 kJ/mol lower in energy. This, together with the virtually barrierless rotation determined from the dynamic NMR studies, indicates that solutions of [**3a**]⁺ contain more than one conformer. The key bond lengths and angles of *anti*-[**3a'**]⁺ are for all intents identical with those of the syn isomer, and there would also therefore appear to be little by way of net reorganization energy in the interconversion of the two conformers. The composition of the β -LUSO and β -HOSO in *anti*-[**3a'**]⁺ is, perhaps surprisingly, almost indistinguishable from that of the syn conformer, with the β -LUSO being largely localized on one ferrocenyl moiety (81%) and the diene (14%) with the β -HOSO again exhibiting more diene-like character (Fc 59%, diene 30%, Fc⁺ 10%) and being somewhat more delocalized.

In order to probe the possible conformational and chemical differences of the mixed-valence complexes [**2,5**-Fc₂-3,4-Ph₂-C₄SiR₂]⁺ further, the complex *anti*-[**3b'**]⁺ was also modeled. The presence of the phenyl substituents made essentially no change to the core geometry of the *cis*-diene-like Fc⁺C=CPhCPh=CFc fragment in comparison with *syn*- or

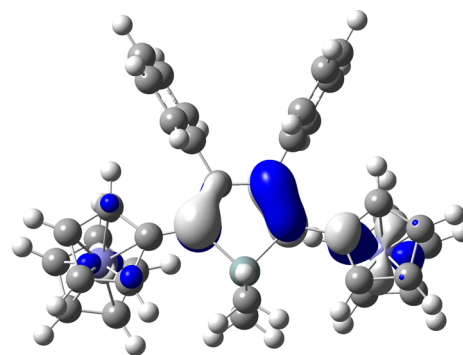
Table 3. Selected Bond Lengths (Å) and Bond and Torsion Angles (deg) from the Crystallographically Determined Structure of **3a** and the Optimized Geometry of Models $[3a']^{n+}$ ($n = 0, 1, 2$)

| | 3a | <i>syn</i> - 3a' | <i>anti</i> - 3a' | <i>syn</i> - $[3a']^+$ | <i>anti</i> - $[3a']^+$ | <i>anti</i> - $[3b']^+$ | <i>syn</i> -T- $[3a']^{2+}$ | <i>anti</i> -T- $[3a']^{2+}$ |
|-------------------------------------|-----------|-------------------------|--------------------------|------------------------|-------------------------|-------------------------|-----------------------------|------------------------------|
| Fe–Cp ₁ ^a | 1.647 | 1.730 | 1.730 | 1.800 | 1.799 | 1.795 | 1.798 | 1.798 |
| Fe–Cp ₆ ^b | 1.648 | 1.730 | 1.732 | 1.731 | 1.731 | 1.730 | 1.796 | 1.798 |
| C1–C2 | 1.462 | 1.467 | 1.467 | 1.445 | 1.445 | 1.447 | 1.457 | 1.458 |
| C2–C3 | 1.360 | 1.380 | 1.380 | 1.395 | 1.394 | 1.391 | 1.386 | 1.386 |
| C3–C4 | 1.498 | 1.507 | 1.507 | 1.487 | 1.487 | 1.490 | 1.497 | 1.498 |
| C4–C5 | 1.359 | 1.380 | 1.380 | 1.390 | 1.390 | 1.387 | 1.386 | 1.386 |
| C5–C6 | 1.463 | 1.467 | 1.467 | 1.458 | 1.458 | 1.457 | 1.457 | 1.458 |
| C2–Si | 1.882 | 1.904 | 1.905 | 1.902 | 1.902 | 1.901 | 1.906 | 1.906 |
| C5–Si | 1.879 | 1.904 | 1.905 | 1.909 | 1.909 | 1.910 | 1.906 | 1.906 |
| C1–C2–C3 | 127.12 | 127.97 | 127.88 | 126.50 | 126.71 | 126.94 | 126.47 | 126.44 |
| C2–C3–C4 | 116.33 | 116.43 | 116.43 | 116.70 | 116.67 | 116.74 | 116.00 | 115.99 |
| C3–C4–C5 | 116.66 | 116.43 | 116.43 | 115.93 | 115.97 | 116.06 | 115.98 | 115.99 |
| C4–C5–C6 | 126.84 | 127.97 | 127.88 | 127.80 | 127.67 | 127.83 | 126.70 | 126.44 |
| C2–Si–C5 | 92.26 | 91.85 | 91.86 | 91.16 | 91.16 | 91.30 | 90.73 | 90.76 |
| CH ₃ –Si–CH ₃ | 109.07 | 111.11 | 110.89 | 111.68 | 111.62 | 111.71 ^c | 112.42 | 112.09 |
| C12–C1–C2–Si | –1.68 | –0.88 | 1.24 | 4.55 | 2.68 | 1.83 | 2.41 | 2.90 |
| C62–C6–C5–Si | 0.11 | 0.84 | 1.25 | 2.40 | 0.88 | 1.14 | 4.39 | 2.91 |

^aCp₁ is the midpoint of the C1–C15 cyclopentadienyl ring. ^bCp₂ is the midpoint of the C6–C65 cyclopentadienyl ring. ^c(*ipso*-C)–Si–(*ipso*-C).

**Figure 8.** Plot of the HOMO of **3a'** (isocontour value ± 0.04 (e/bohr^3)^{1/2}).**Figure 9.** Plot of the β -LUSO of $[3a']^+$ (isocontour value ± 0.04 (e/bohr^3)^{1/2}).

anti- $[3a']^+$ (Table 3), although the ferrocenyls are slightly distorted from coplanarity (FeCp₁...FeCp₂: *anti*- $[3b']^+$, -172.00° ; *anti*- $[3a']^+$, -175.25° Me₂). This minor geometric variation and the impact on the electronic structure are potentially interesting with regards to the suggestion of a degree of attenuation of the coupling between the ferrocenyl moieties through the 1,1,3,4-tetraphenylsilacyclopentadiene scaffold of $[3b]^+$ vs $[3a]^+$ made on the basis of the electrochemical and near-IR data. While the β -LUSO of this lowest energy geometry of *anti*- $[3b']^+$ exhibits the same composition as in *syn*- and *anti*- $[3a']^+$ (Fc⁺ 80%, diene 15%,

**Figure 10.** Plot of the β -HOSO of $[3a']^+$ (isocontour value ± 0.04 (e/bohr^3)^{1/2}).

Fc 4%), the diene contribution to the β -HOSO in *anti*- $[3b']^+$ is somewhat smaller (Fc 65%, diene 25%, Fc⁺ 8%). Given that the IVCT transition is approximated in terms of the β -HOSO \rightarrow β -LUSO transition, the lower overlap between these orbitals may be responsible for the modestly weaker coupling. Such suggestions must be tempered against the relatively high barriers to rotation about the C1–C2 and C5–C6 bonds determined by dynamic NMR arising from the T-shaped π – π interactions, taken in light of the likely conformational distribution in solution. The notion that the SiPh₂ moiety presents a steric barrier to the optimal coplanar arrangement of the ferrocenyl and silacyclic moieties would be consistent with the modestly weaker coupling observed in $[3b]^+$ in comparison to that in $[3a]^+$.

As an aside, we note that at the level of theory employed, a local minimum with a *symmetric* (i.e., delocalized or class III) electronic structure was also found for *anti*- $[3a']^+$, which differs only slightly in individual bond lengths and is only 14 kJ/mol higher in energy than the class II form described above (Supporting Information). Given the well-known overestimation of delocalized electronic structures from the B3LYP functional, it is not appropriate to base any substantive comment on the apparently low energy difference between the class II and class III forms of *anti*- $[3a']^+$. However, the

point to note is not that the B3LYP hybrid functional identifies a structure with a delocalized electronic structure but rather that there are only very subtle changes in bond length required to pass between class II and class III in these complexes (a point that is implicit in the thermal barrier to electron transfer associated with class II complexes).

The dication $\text{syn-}[3\mathbf{a}']^{2+}$ proved to be substantially more stable in the triplet (or high-spin, HS) ground state ($\Delta E_{\text{T-S}}: -118.6 \text{ kJ/mol } [3']^{2+}$), and consequently the discussions here are restricted to this state. The molecular geometry of HS- $[3\mathbf{a}']^{2+}$ reflects the homovalent nature of the two iron centers, with essentially identical geometric parameters observed in each half of the dication, and a restoration of the more pronounced bond-length alternation in the *cis*-diene backbone (Table 3). The dication is therefore well described as two ferrocenium moieties pendant to the silacycle.

CONCLUSION

The synthesis of 2,5-diferrocenyl-3,4-diphenyl siloles bearing methyl (**3a**) or phenyl (**3b**) groups at the silicon atom are realized by a reductive cyclization reaction of dimethyl- or diphenylbis(phenylethynyl)silane with lithium naphthalenide. The ferrocenyl substituents are introduced to the silole ring by Negishi C,C cross-coupling reactions, whereas the silole ring either was applied as a vinyl halogenide or as a zinc organic component. Electrochemical investigations showed that the ferrocenyl units of both synthesized siloles can be oxidized separately. In contrast to findings among the series of aromatic diferrocenyl five-membered heterocycles,^{15,18,19,44,45} the more electron rich siloles showed a lower redox separation between the individual ferrocenyl oxidation processes. Spectroelectrochemical investigations confirmed electron charge transfer interactions between the individual ferrocenyl termini across the silole linking unit, which are comparable to those found in diferrocenyl phosphole¹⁵ or diferrocenyl *cis*-butadiene systems,⁴³ arguing that the C₄ chain at the molecule's backbone mediates the electronic coupling. Molecules $[3\mathbf{a},\mathbf{b}]^+$ can be characterized as moderate or moderate to weakly coupled class II species according to Robin and Day. Despite being more electron rich, **3b**⁺ showed less intense IVCT absorptions than the dimethylsilole $[3\mathbf{a}]^+$, which may be due to steric interactions. DFT calculations are consistent with the class II mixed valence description of $[3\mathbf{a},\mathbf{b}]^+$, with the apparent low differences in energy between *syn* and *anti* conformations suggesting a distribution of molecular geometries, and hence variation in electronic coupling, in solution.

EXPERIMENTAL SECTION

General Conditions. All reactions were carried out under an atmosphere of argon using standard Schlenk techniques. Tetrahydrofuran was purified by distillation from sodium/benzophenone ketyl. For column chromatography, alumina with a particle size of 90 μm (standard, Merck KGaA) was used.

Reagents. 2,5-Dibromo-1,1-dimethyl-3,4-diphenyl-1H-silole⁵⁹ and diphenylbis(phenylethynyl)silane⁶⁰ were prepared in analogy to published procedures. $[\text{N}^n\text{Bu}_4][\text{B}(\text{C}_6\text{F}_5)_4]$ was prepared by methathesis of lithium tetrakis(pentafluorophenyl)borate etherate (Boulder Scientific) with tetra-*n*-butylammonium bromide according to ref 35. $[\text{P}(\text{C}_4\text{H}_9)_2\text{C}(\text{CH}_3)_2\text{CH}_2\text{Pd}(\mu\text{-Cl})_2]$ ^{61,62} and iodoferrrocene^{63,64} were prepared according to published procedures. All other chemicals were purchased from commercial suppliers and were used as received.

Instrumentation. Infrared spectra were recorded using a FT-Nicolet IR 200 equipment. The ¹H NMR spectra were recorded with a Bruker Avance III 500 spectrometer operating at 500.303 MHz in the

Fourier transform mode; the ¹³C{¹H} NMR spectra were recorded at 125.800 MHz. Chemical shifts are reported in ppm downfield from tetramethylsilane with the solvent as reference signal (¹H NMR, $\delta(\text{CHCl}_3)$ 7.26 ppm; ¹³C{¹H} NMR, $\delta(\text{CHCl}_3) = \delta(\text{CDCl}_3)$ 77.16 ppm; ²⁹Si{¹H} NMR, $\delta(\text{TMS})$ 0.00 ppm). The melting points were determined using a Gallenkamp MFB 595 010 M melting point apparatus. Elemental analyses were performed with a Thermo FlashEA 1112 Series instrument. High-resolution mass spectra were recorded using a micrOTOF QII Bruker Daltonite workstation. UV-vis spectra were recorded with a THERMO Genesis 6 spectrometer.

X-ray Diffraction. Data were collected with an Oxford Gemini S diffractometer at 110 K using Mo K α ($\lambda = 0.71073 \text{ \AA}$) radiation. The structures were solved by direct methods and refined by full-matrix least-squares procedures on F^2 .^{65,66} All non-hydrogen atoms were refined anisotropically, and a riding model was employed in the treatment of the hydrogen atom positions.

Electrochemistry. Electrochemical measurements on 1.0 mmol L⁻¹ solutions of the analytes in dry, air-free dichloromethane containing 0.1 mol L⁻¹ of $[\text{N}^n\text{Bu}_4][\text{B}(\text{C}_6\text{F}_5)_4]$ as supporting electrolyte were conducted under a blanket of purified argon at 25 °C utilizing a Radiometer Voltalab PGZ 100 electrochemical workstation interfaced with a personal computer. A three-electrode cell, which utilized a Pt auxiliary electrode, a glassy-carbon working electrode (surface area 0.031 cm²), and an Ag/Ag⁺ (0.01 mol·L⁻¹ AgNO₃) reference electrode mounted on a Luggin capillary, was used. The working electrode was pretreated by polishing on a Buehler microcloth first with a 1 μm and then a 1/4 μm diamond paste. The reference electrode was constructed from a silver wire inserted into a solution of 0.01 mol L⁻¹ [AgNO₃] and 0.1 mol L⁻¹ $[\text{N}^n\text{Bu}_4][\text{B}(\text{C}_6\text{F}_5)_4]$ in acetonitrile, in a Luggin capillary with a Vycor tip. This Luggin capillary was inserted into a second Luggin capillary with a Vycor tip filled with a 0.1 mol L⁻¹ $[\text{N}^n\text{Bu}_4][\text{B}(\text{C}_6\text{F}_5)_4]$ solution in dichloromethane.³⁶ Successive experiments under the same experimental conditions showed that all formal reduction and oxidation potentials were reproducible within 5 mV. Experimentally, potentials were referenced against an Ag/Ag⁺ reference electrode, but results are presented referenced to ferrocene as an internal standard, as required by IUPAC.⁴² When decamethylferrocene was used as an internal standard, the experimentally measured potential was converted into E vs FcH/FcH⁺ by addition of -619 mV.⁶⁷ Data were then manipulated on a Microsoft Excel worksheet to set the formal reduction potentials of the FcH/FcH⁺ couple to $\Delta E^{\circ\prime} = 0.0 \text{ V}$. Ferrocene itself showed a redox potential of 220 mV vs Ag/Ag⁺ ($\Delta E_p = 61 \text{ mV}$) within our measurements.^{68,69} The cyclic voltammograms, which are depicted (Figure 4), were taken after typically two scans and are considered to be steady-state cyclic voltammograms in which the signal pattern does not differ from the initial sweep.

Spectroelectrochemistry. UV-vis-near-IR measurements were carried out in an OTTE (optically thin layer electrochemistry) cell with quartz windows similar to that described previously⁷⁰ in dry dichloromethane solutions containing 2.0 mmol L⁻¹ analyte and 0.1 mol L⁻¹ of $[\text{N}^n\text{Bu}_4][\text{B}(\text{C}_6\text{F}_5)_4]$ as supporting electrolyte using a Varian Cary 5000 spectrophotometer at 25 °C. The Pt-mesh working electrode, the AgCl-coated Ag wire reference electrode, and the Pt-mesh auxiliary electrode were melt-sealed into a polyethylene spacer. The values obtained by deconvolution could be reproduced within $\epsilon_{\text{max}} = 100 \text{ L mol}^{-1} \text{ cm}^{-1}$, $\nu_{\text{max}} = 50 \text{ cm}^{-1}$, and $\Delta\nu_{1/2} = 50 \text{ cm}^{-1}$. Between the spectroscopic measurements the applied potentials were increased in a stepwise fashion using a step height of 25, 50, or 100 mV. At the end of the measurements the analyte was reduced at -400 mV for 30 min and an additional spectrum was recorded to prove the reversibility of the oxidations.

Computational Chemistry. Calculations were carried out with the Gaussian 09⁷¹ package, with GaussView 5.0.8⁷² and GaussSum3.0⁷³ used to further analyze the results. All geometries were optimized with the B3LYP functional, using the LAN2DZ basis set on Fe and 6-31G** on all other atoms, with a CPCM (dichloromethane) solvent model. All optimized geometries were confirmed as true minima by the absence of imaginary frequencies.

Synthesis of 2,5-Diferrocenyl-1,1-dimethyl-3,4-diphenyl-1H-silole (3a). To a solution of 9.52 mmol of ferrocenyl zinc chloride in 40 mL of tetrahydrofuran, prepared by monolithiation of ferrocene (1.95 g, 10.47 mmol)⁷⁴ followed by addition of [ZnCl₂·2thf] (4.23 g, 15.08 mmol) at -80 °C, was added 2,5-dibromo-1,1-dimethyl-3,4-diphenylsilole (2.0 g, 10.47 mmol) in a single portion at 25 °C. To the solution was added 16.3 mg (24 μmol) of [P(^tC₄H₉)₂C(CH₃)₂CH₂Pd(μ-Cl)]₂ and the mixture was stirred for 2 days at 80 °C. After evaporation of all volatiles, the precipitate was dissolved in 70 mL of diethyl ether and washed three times with 60 mL portions of water. The organic phase was dried over MgSO₄, and all volatiles were removed. The remaining crude solid was purified by column chromatography (column size 20 × 4 cm, on alumina) using a 2/1 (v/v) *n*-hexane/dichloromethane mixture as eluent. All volatiles were removed under reduced pressure, and the wine red solid was crystallized from *n*-hexane at 68 °C. Yield: 35% (based on 2,5-dibromo-1,1-dimethyl-3,4-diphenylsilole). Anal. Calcd for C₃₈H₃₄Fe₂Si (*M* = 630.45: C, 72.39; H, 5.44. Found: C, 71.89; H, 5.38. Mp: 275 °C dec. IR (KBr, in cm⁻¹): 3087 (w), 3076 (m), 3056 (m), 3022 (m), 2947 (w), 2923 (w), 1682 (w), 1442 (m), 1241 (s), 1106 (s) 1000 (s), 793 (s), 745 (s), 702 (s), 506 (s). ¹H NMR (CDCl₃, δ in ppm): 0.73 (s, 6H, CH₃), 3.71 (pt, *J*_{HH} = 1.89 Hz, 4H, C₅H₄), 4.06 (s, 10H, C₅H₅), 4.10 (pt, *J*_{HH} = 1.89 Hz, 4H, C₅H₄), 6.96–7.00 (m, 4H, *o*-C₆H₅), 7.09–7.14 (m, 2H, *p*-C₆H₅), 7.18–7.22 (m, 4H, *m*-C₆H₅). ¹³C{¹H} NMR (CDCl₃, δ in ppm): -1.0 (CH₃), 68.6 (C₅H₄), 68.7 (C₅H₄), 69.5 (C₅H₅), 83.3 (*i*C-C₅H₄), 126.4 (*o*-C₆H₅), 128.0 (*m*-C₆H₅), 129.3 (*p*-C₆H₅), 134.8 (2,5-C₄Si), 141.6 (*i*-C₆H₅), 152.6 (3,4-C₄Si). ²⁹Si{¹H} NMR (CDCl₃, δ in ppm): 5.70 (s, Si). UV-vis: 391 nm (12057 L mol⁻¹ cm⁻¹), 507 nm (5073 L mol⁻¹ cm⁻¹). HRMS (ESI-TOF, *m/z*): calcd for C₃₈H₃₄Fe₂Si 630.1129, found 630.1198 [M]⁺. Crystal data for 3b: C₃₈H₃₄Fe₂Si, *M*_r = 630.44, orthorhombic, *Pbc*a, λ = 0.71073 Å, *a* = 13.036(5) Å, *b* = 19.934(5) Å, *c* = 22.598(5) Å, *V* = 5872(3) Å³, *Z* = 8, ρ_{calcd} = 1.426 g m⁻³, μ = 1.023 mm⁻¹, *T* = 110 K, θ range 3.13–26.00°, 56340 reflections collected, 5734 independent reflections (*R*_{int} = 0.0338), *R*₁ = 0.0258, *wR*₂ = 0.0635 (*I* > 2σ(*I*)).

Synthesis of 2,5-Diferrocenyl-1,1,3,4-tetraphenyl-1H-silole (3b). Lithium naphthalene was prepared by stirring 84.5 mg (12.18 mmol) of lithium with 1.56 g (12.18 mmol) of naphthalene in 10 mL of dry tetrahydrofuran at room temperature for 18 h. To this solution was added 1.17 g (3.04 mmol) of diphenylbis(phenylethynyl)silane in a single portion, and the mixture was stirred for 1 h. Afterward, 3.41 g (12.18 mmol) of [ZnCl₂·2thf] was added in a single portion at 0 °C, 10 mL of dry tetrahydrofuran was added, and the mixture was stirred again for 1 h. Iodoferrocene (1.97 g (6.33 mmol)) and 12 mg (17.5 μmol) of [P(^tC₄H₉)₂C(CH₃)₂CH₂Pd(μ-Cl)]₂ were added, and the reaction mixture was stirred for 2 days at 80 °C. After evaporation of all volatiles, the solid material was dissolved in 40 mL of diethyl ether and washed three times with 30 mL portions of water. The organic phase was dried over MgSO₄, and all volatiles were removed. The remaining crude solid was purified by column chromatography (column size 20 × 2 cm, on alumina) using a 4/1 (v/v) *n*-hexane/dichloromethane mixture as eluent. All volatiles were removed under reduced pressure, and the wine red solid was crystallized from *n*-hexane at 68 °C. Yield: 12% (based on diphenylbis(phenylethynyl)silane). C₄₈H₃₈Fe₂Si (*M* = 754.59). Mp: 280 °C dec. IR (KBr, in cm⁻¹): 3089 (w), 3070 (m), 3048 (m), 3021 (m), 1594 (w), 1557 (m), 1483 (m), 1429 (m), 1267 (s), 1112 (s), 1105 (s) 1000 (s), 819 (s), 770 (s) 735 (s), 706 (s), 504 (s). ¹H NMR (CDCl₃, δ in ppm): 3.52 (s, 10H, C₅H₅), 3.57 (pt, *J*_{HH} = 1.89 Hz, 4H, C₅H₄), 3.95 (pt, *J*_{HH} = 1.89 Hz, 4H, C₅H₄), 7.06–7.09 (m, 4H, *o*-C₆H₅), 7.13–7.17 (m, 2H, *p*-C₆H₅), 7.22–7.26 (m, 4H, *m*-C₆H₅), 7.52–7.55 (m, 6H, Si-C₆H₅), 8.00–8.03 (m, 4H, Si-C₆H₅). ¹³C{¹H} NMR (CDCl₃, δ in ppm): 68.6 (C₅H₄), 69.5 (C₅H₅), 69.5 (C₅H₄), 82.8 (*i*C-C₅H₄), 126.6 (C-*o*-C₆H₅), 128.1 (C-C₆H₅), 128.6 (Si-C₆H₅), 129.4 (C-C₆H₅), 130.5 (Si-C₆H₅), 133.5 (C₆H₅), 133.8 (C₆H₅), 136.8 (Si-C₆H₅), 141.6 (*i*-C₆H₅), 154.8 (3,4-C₄Si). UV-vis: 398 nm (11846 L mol⁻¹ cm⁻¹), 523 nm (5297 L mol⁻¹ cm⁻¹). HRMS (ESI-TOF, *m/z*): calcd for C₄₈H₃₈Fe₂Si 754.1442, found 754.1425 [M]⁺. Crystal data for 3b: C₄₈H₃₈Fe₂Si·2CH₂Cl₂, *M*_r = 924.42, monoclinic, *P2*/*n*, *a* = 13.1115(4)

Å, *b* = 10.8183(4) Å, *c* = 14.8040(4) Å, *V* = 2073.56(12) Å³, *Z* = 2, ρ_{calcd} = 1.481 g m⁻³, μ = 1.023 mm⁻¹, *T* = 110 K, θ range 2.942–24.997°, 8460 reflections collected, 3644 independent reflections (*R*_{int} = 0.0205), *R*₁ = 0.0520, *wR*₂ = 0.1284 (*I* > 2σ(*I*)).

■ ASSOCIATED CONTENT

Supporting Information

Figures, tables, and .xyz and CIF files giving further (spectro)electrochemical spectra, computational data, and crystallographic data for 3a,b. This material is available free of charge via the Internet at <http://pubs.acs.org>. Crystallographic data for 3a,b are also available from the Cambridge Crystallographic Database as file numbers CCDC 981390 (3a) and 981391 (3b).

■ AUTHOR INFORMATION

Corresponding Author

*H.L.: e-mail, heinrich.lang@chemie.tu-chemnitz.de; tel, +49 (0)371-531-21210; fax, +49 (0)371-531-21219.

Author Contributions

§Author to whom correspondence pertaining to the calculations should be directed.

Notes

The authors declare no competing financial interest.

■ ACKNOWLEDGMENTS

We thank Dr. Holm Petzold for assistance with the dynamic NMR measurements. We are grateful to the Fonds der Chemischen Industrie for generous financial support. M.K. thanks the Fonds der Chemischen Industrie for a Chemiefonds fellowship. P.J.L. holds an Australian Research Council Future Fellowship (FT120100073) and gratefully acknowledges financial support for this work from the ARC (DP140100855).

■ REFERENCES

- (1) Hongt, S. Y.; Marynick, D. S. *Macromolecules* **1995**, *28*, 4991–4995.
- (2) Lu, G.; Usta, H.; Risko, C.; Wang, L.; Facchetti, A.; Ratner, M. A.; Marks, T. J. *J. Am. Chem. Soc.* **2008**, *130*, 7670–7685.
- (3) Hong, Y.-R.; Wong, H.-K.; Moh, L. C. H.; Tan, H.-S.; Chen, Z.-K. *Chem. Commun.* **2011**, *47*, 4920–4922.
- (4) Wang, F.; Luo, J.; Yang, K.; Chen, J.; Huang, F.; Cao, Y. *Macromolecules* **2005**, *38*, 2253–2260.
- (5) Tamao, K.; Yamaguchi, S.; Shiozaki, M.; Nakawaga, Y.; Ito, Y. *J. Am. Chem. Soc.* **1992**, *114*, 5867–5869.
- (6) Ma, J.; Li, S.; Jiang, Y. *Macromolecules* **2002**, *35*, 1109–1115.
- (7) Yamaguchi, Y.; Shioya, J. *Mol. Eng.* **1993**, 339–347.
- (8) Frapper, G.; Kertesz, M. *Organometallics* **1992**, *11*, 3178–3184.
- (9) Zotti, G.; Martina, S.; Wegner, G.; Schlüter, A.-D. *Adv. Mater.* **1992**, 798–801.
- (10) Roncali, J. *Chem. Rev.* **1997**, *97*, 173–206.
- (11) Zhao, Z.; Liu, D.; Mahtab, F.; Xin, L.; Shen, Z.; Yu, Y.; Chan, C. Y. K.; Lu, P.; Lam, J. W. Y.; Sung, H. H. Y.; Williams, I. D.; Yang, B.; Ma, Y.; Tang, B. Z. *Chem. Eur. J.* **2011**, *17*, 5998–6008.
- (12) Li, C. B.; Yang, G. X.; Huang, Z. H.; Xin, Y.; Wang, C.; Yuan, J. H. *Pigm. Resin Technol.* **2009**, *38*, 387–391.
- (13) Murata, H.; Kafafi, Z. H.; Uchida, M. *Appl. Phys. Lett.* **2002**, *80*, 189.
- (14) Chen, H. Y.; Lam, W. Y.; Luo, J. D.; Ho, Y. L.; Tang, B. Z.; Zhu, D. B.; Wong, M.; Kwok, H. S. *Appl. Phys. Lett.* **2002**, *81*, 574.
- (15) Miesel, D.; Hildebrandt, A.; Korb, M.; Low, P. J.; Lang, H. *Organometallics* **2013**, *32*, 2993–3002.
- (16) Kaleta, K.; Strehler, F.; Hildebrandt, A.; Beweries, T.; Arndt, P.; Rüffer, T.; Spannenberg, A.; Lang, H.; Rosenthal, U. *Chem. Eur. J.* **2012**, *18*, 12672–12680.

- (17) Kaleta, K.; Hildebrandt, A.; Strehler, F.; Arndt, P.; Jiao, H.; Spannenberg, A.; Lang, H.; Rosenthal, U. *Angew. Chem.* **2011**, *123*, 11444–11448.
- (18) Hildebrandt, A.; Lehrich, S. W.; Schaarschmidt, D.; Jaeschke, R.; Schreiter, K.; Spange, S.; Lang, H. *Eur. J. Inorg. Chem.* **2012**, 1114–1121.
- (19) Hildebrandt, A.; Schaarschmidt, D.; Lang, H. *Organometallics* **2011**, *30*, 556–563.
- (20) Speck, M.; Schaarschmidt, D.; Lang, H. *Organometallics* **2012**, 1975–1982.
- (21) Hildebrandt, A.; Pfaff, U.; Lang, H. *Rev. Inorg. Chem.* **2011**, *31*, 111–141.
- (22) Hildebrandt, A.; Schaarschmidt, D.; van As, L.; Swarts, J. C.; Lang, H. *Inorg. Chim. Acta* **2011**, *374*, 112–118.
- (23) Pfaff, U.; Hildebrandt, A.; Schaarschmidt, D.; Ruffer, T.; Low, P. J. *Organometallics* **2013**, *32*, 6106–6117.
- (24) Günther, H. *Angew. Chem., Int. Ed. Engl.* **1972**, *1*, 861–874.
- (25) Vignau, L.; Janot, J. *New J. Chem.* **2004**, 1086–1090.
- (26) Sinnokrot, M. O.; Valeev, E. F.; Sherrill, C. D. *J. Am. Chem. Soc.* **2002**, *124*, 10887–10893.
- (27) Zhao, Y.; Truhlar, D. G. *J. Phys. Chem. A* **2005**, *109*, 4209–4212.
- (28) Chen, J.; Law, C. C. W.; Lam, J. W. Y.; Dong, Y.; Lo, S. M. F.; Williams, I. D.; Zhu, D.; Tang, B. Z. *Chem. Mater.* **2003**, *15*, 1535–1546.
- (29) Tracy, H. J.; Mullin, J. L.; Klooster, W. T.; Martin, J. a; Haug, J.; Wallace, S.; Rudloe, I.; Watts, K. *Inorg. Chem.* **2005**, *44*, 2003–2011.
- (30) Yu, G.; Yin, S.; Liu, Y.; Chen, J.; Xu, X.; Sun, X.; Ma, D.; Zhan, X.; Peng, Q.; Shuai, Z.; Tang, B.; Zhu, D.; Fang, W.; Luo, Y. *J. Am. Chem. Soc.* **2005**, *127*, 6335–6346.
- (31) Ferman, J.; Kakareka, J. P.; Klooster, W. T.; Mullin, J. L.; Quattrucci, J.; Ricci, J. S.; Tracy, H. J.; Vining, W. J.; Wallace, S. *Inorg. Chem.* **1999**, *38*, 2464–2472.
- (32) Günther, H. *NMR spectroscopy: basic principles, concepts, and applications in chemistry*, 2nd ed.; Wiley: New York, 1996.
- (33) Neumann, R. C.; Jonas, V. *J. Org. Chem.* **1974**, *39*, 925–929.
- (34) Barrière, F.; Geiger, W. E. *J. Am. Chem. Soc.* **2006**, *128*, 3980–3989.
- (35) LeSuer, R. J.; Buttolph, C.; Geiger, W. E. *Anal. Chem.* **2004**, *76*, 6395–6401.
- (36) Gericke, H. J.; Barnard, N. I.; Erasmus, E.; Swarts, J. C.; Cook, M. J.; Aquino, M. a. S. *Inorg. Chim. Acta* **2010**, *363*, 2222–2232.
- (37) Hildebrandt, A.; Lehrich, S. W.; Schaarschmidt, D.; Jaeschke, R.; Schreiter, K.; Spange, S.; Lang, H. *Eur. J. Inorg. Chem.* **2012**, 2012, 1114–1121.
- (38) Pfaff, U.; Hildebrandt, A.; Schaarschmidt, D.; Hahn, T.; Liebing, S.; Kortus, J.; Lang, H. *Organometallics* **2012**, *31*, 6761–6771.
- (39) Solntsev, P. V.; Dudkin, S. V.; Sabin, J. R.; Nemykin, V. N. *Organometallics* **2011**, *30*, 3037–3046.
- (40) Goetsch, W. R.; Solntsev, P. V.; Stappen, C.; Van Purchel, A. A.; Dudkin, S. V.; Nemykin, V. N. *Organometallics* **2014**, *33*, 145–157.
- (41) Chong, D.; Slote, J.; Geiger, W. E. *J. Electroanal. Chem.* **2009**, *630*, 28–34.
- (42) Gritzner, G.; Kuta, J. *Pure Appl. Chem.* **1984**, *56*, 461–466.
- (43) Li, Y.; Josowicz, M.; Tolbert, L. M. *J. Am. Chem. Soc.* **2010**, *132*, 10374–10382.
- (44) Hildebrandt, A.; Schaarschmidt, D.; Claus, R.; Lang, H. *Inorg. Chem.* **2011**, *50*, 10623–10632.
- (45) Speck, M.; Claus, R.; Hildebrandt, A.; Ru, T.; Erasmus, E.; As, L. Van; Swarts, J. C.; Lang, H. *Organometallics* **2012**, 6373–6380.
- (46) Faustov, V. I.; Egorov, M. P.; Nefedov, M.; Molin, Y. N. *Phys. Chem. Chem. Phys.* **2000**, *2*, 4293–4297.
- (47) Göransson, E.; Emanuelsson, R.; Jorner, K.; Markle, T. F.; Hammarström, L.; Ottosson, H. *Chem. Sci.* **2013**, *4*, 3522.
- (48) Tibbelin, J.; Wallner, A.; Emanuelsson, R.; Heijkenskjöld, F.; Rosenberg, M.; Yamazaki, K.; Nauroozi, D.; Karlsson, L.; Feifel, R.; Pettersson, R.; Baumgartner, J.; Ott, S.; Ottosson, H. *Chem. Sci.* **2014**, *5*, 360.
- (49) Emanuelsson, R.; Wallner, A.; Ng, E. M.; Smith, J. R.; Nauroozi, D.; Ott, S.; Ottosson, H. *Angew. Chem., Int. Ed.* **2013**, *52*, 983–987.
- (50) D'Alessandro, D. M.; Keene, F. R. *Dalton Trans.* **2004**, 3950–3954.
- (51) Low, P. J.; Brown, N. J. *J. Cluster Sci.* **2010**, *21*, 235–278.
- (52) Hildebrandt, A.; Ruffer, T.; Erasmus, E.; Swarts, J. C.; Lang, H. *Organometallics* **2010**, *29*, 4900–4905.
- (53) Hildebrandt, A.; Lang, H. *Dalton Trans.* **2011**, *40*, 11831–11837.
- (54) Hildebrandt, A.; Lang, H. *Organometallics* **2013**, *32*, 5640–5653.
- (55) D'Alessandro, D. M.; Keene, F. R. *Chem. Soc. Rev.* **2006**, *35*, 424–440.
- (56) Brunschwig, B. S.; Creutz, C.; Sutin, N. *Chem. Soc. Rev.* **2002**, *31*, 168–184.
- (57) Lapinte, C. *J. Organomet. Chem.* **2008**, *693*, 793–801.
- (58) Mücke, P.; Linseis, M.; Zális, S.; Winter, R. F. *Inorg. Chim. Acta* **2011**, *374*, 36–50.
- (59) Tamao, K.; Yamaguchi, S.; Shiro, M. *J. Am. Chem. Soc.* **1994**, *117*, 11715–11722.
- (60) Morra, N. A.; Pagenkopf, B. L. *Org. Synth.* **2008**, *85*, 53–63.
- (61) Clark, H. C.; Goel, A. B.; Goel, R. G.; Goel, S.; Ogini, W. O. *Inorg. Chim. Acta* **1978**, *31*, L441–442.
- (62) Goel, A. B.; Goel, S. *Inorg. Chim. Acta* **1985**, *98*, 67–70.
- (63) Goeltz, J. C.; Kubiak, C. P. *Organometallics* **2011**, *30*, 3908–3910.
- (64) Inkpen, M. S.; Du, S.; Driver, M.; Albrecht, T.; Long, N. J. *Dalton Trans.* **2013**, *42*, 2813–2816.
- (65) Sheldrick, G. M. *Acta Crystallogr., Sect. A: Found. Crystallogr.* **1990**, *46*, 467–473.
- (66) Sheldrick, G. M. *SHELXL-97, Program for Crystal Structure Refinement*; University of Göttingen, Göttingen, Germany, 1997.
- (67) Nafady, A.; Geiger, W. E. *Organometallics* **2008**, 5624–5631.
- (68) Ruiz, J. A.; Daniel, M.-C.; Astruc, D. *Can. J. Chem.* **2006**, *84*, 288–299.
- (69) Ruiz, J.; Astruc, D. *C. R. Acad. Sci., Ser. IIC: Chim.* **1998**, *1*, 21–27.
- (70) Krejciak, M.; Danek, M.; Hartl, F. *J. Electroanal. Chem.* **1991**, *317*, 179–187.
- (71) Frisch, M. J., et al. *Gaussian 09, Revision D.01*; Gaussian Inc., Wallingford, CT, 2009.
- (72) Dennington, R.; Keith, T.; Millam, J. *GaussView 5.0.8*; Semichem Inc., Shawnee Mission, KS, 2009.
- (73) O'Boyle, N. M.; Tenderholt, A. L.; Langner, K. M. *J. Comput. Chem.* **2008**, *29*, 839–845.
- (74) Sanders, R.; Mueller-Westerhoff, U. T. *J. Organomet. Chem.* **1996**, *S12*, 219–224.